# Refinement of a Homology Model of the μ-Opioid Receptor Using Distance Constraints from Intrinsic and Engineered Zinc-Binding Sites †

**4 AUTHORS,** INCLUDING:

Carol B Fowler
U.S. Department of Veterans Affairs
**34** PUBLICATIONS **526** CITATIONS

SEE PROFILE

Irina D Pogozheva
University of Michigan
**64** PUBLICATIONS **2,014** CITATIONS

SEE PROFILE

Henry I Mosberg
University of Michigan
**186** PUBLICATIONS **7,208** CITATIONS

SEE PROFILE

# Refinement of a Homology Model of the μ-Opioid Receptor Using Distance Constraints from Intrinsic and Engineered Zinc-Binding Sites[†]

Carol B. Fowler,[‡] Irina D. Pogozheva,[‡] Harry LeVine, III,[§] and Henry I. Mosberg*,[‡]

*Department of Medicinal Chemistry, University of Michigan, 428 Church Street, Ann Arbor, Michigan 48109-1065, and
Department of Molecular and Cellular Biochemistry, Chandler School of Medicine and the Center on Aging,
University of Kentucky, Lexington, Kentucky 40536*

ABSTRACT: Publication of the rhodopsin X-ray structure has facilitated the development of homology models of other G protein-coupled receptors. However, possible shifts of transmembrane (TM) α helices, expected variations in helical distortions, and differences in loop size necessitate experimental verification of these comparative models. To refine a rhodopsin-based homology model of the μ-opioid receptor (MOR), we experimentally determined structural-distance constraints from intrinsic and engineered metal-binding sites in the rat MOR. Investigating the relatively high intrinsic affinity of MOR for $Zn^{2+}$ ($IC_{50} \sim 30 \mu M$), we observed that mutation of $His^{319}$ (TM7) abolished $Zn^{2+}$ inhibition of ligand binding, while mutation of $Asp^{216}$ (extracellular loop 2) decreased the effect of $Zn^{2+}$, suggesting these residues participate in the intrinsic $Zn^{2+}$-binding center of MOR. To verify the relative orientation of TM5 and TM6 and to examine whether a rhodopsin-like α aneurism is present in TM5, we engineered $Zn^{2+}$-binding centers by mutating residues of TM5 and TM6 to Cys or His, making use of the native $His^{297}$ in TM6 as an additional $Zn^{2+}$-coordination site. Inhibition of opioid ligand binding by $Zn^{2+}$ suggests that residues $Ile^{234}$ and $Phe^{237}$ in TM5 face the binding-site crevice and form a metal-binding center with $His^{297}$ and $Val^{300}$ in TM6. This observation is inconsistent with a rhodopsin-like structure, which would locate $Ile^{234}$ on the lipid-exposed side of TM5, too distant from other residues making up the $Zn^{2+}$-binding site. Subsequent distance geometry refinement of the MOR model indicates that the rhodopsin-like α aneurism is likely absent in TM2 but present in TM5.

The μ-, δ-, and κ-opioid receptors are members of the rhodopsin-like G protein-coupled receptor (GPCR)[1] superfamily, which transduce chemical and optical signals through the cell membrane by activating intracellular G proteins. The opioid receptors are negatively coupled to cAMP production mainly through $G_{i,o}$ (*1*) and play important roles in the modulation of pain perception and mood regulation. Clinically, opiates such as morphine are used as analgesics but are among the most widely abused drugs, principally because of their reinforcing euphoric effects, which are mediated primarily through the μ receptor (*2*).

Except for the recently crystallized rhodopsin (*3*), structural data on individual GPCRs are limited; therefore, theoretical modeling remains an important tool for structure−function analysis of these receptors. Early computational models of GPCRs were largely based upon low-resolution electron density maps of rhodopsin or high-resolution bacteriohodopsin structures (*4*). During the mid to late 1990s, several models of opioid receptors were proposed using different computational techniques (*5−11*). We developed at that time a computational approach for modeling the transmembrane 7 α-helical bundle of GPCRs that entailed an iterative distance geometry refinement with an evolving system of interhelical hydrogen-bonding constraints (*12*) and applied it to the modeling of ∼30 different rhodopsin-like GPCRs, including the μ-, δ-, and κ-opioid receptors (*13*, *14*). The validity of our approach was confirmed by the publication of the crystal structure of rhodopsin (*3*, *15*), which is in very close agreement with our ab initio model (*12*), demonstrating a root-mean-square deviation (RMSD) of 2.88 Å for 186 Cα atoms.

The publication of the rhodopsin crystal structure has made homology modeling of receptors from the rhodopsin-like family possible (*16−18*), and several opioid receptor models based on the rhodopsin template have subsequently been produced (*19−23*). It is known that the accuracy of comparative modeling is highly dependent on the sequence identity between the target sequence of interest and the template sequence (*24*, *25*). The opioid receptor sequences, while close in size to the rhodopsin sequence especially for TM segments and interhelical loops, have only ∼20% identity for all residues and ∼29% identity in TM segments. Therefore, modeling errors and structural deviation between opioid receptors and the rhodopsin structure can be expected. The major errors in homology modeling are associated with misalignments in the evolutionarily conserved core, helix distortions, shifts of core segments, side-chain packing, and

loop-modeling errors (*24, 25*). Misalignment, which is frequent in areas of low sequence identity and in regions of distortions of secondary structure, is especially detrimental for accurate structural modeling (*26*).

The structural core of rhodopsin consists of seven TM $\alpha$ helices, a $\beta$ hairpin in extracellular loop 2 (EL2) attached by the conserved disulfide to TM3, and the peripheral helix 8, which is conserved in the majority of rhodopsin-like receptors, as evidenced from multiple sequence alignments (*19*). The N- and C-terminal fragments and the interhelical loops represent variable structural elements. Helix irregularities are often present in the structures of $\alpha$-helical membrane proteins, but their positions can vary among homologous proteins (*27*). Examination of the rhodopsin X-ray structure reveals a number of helix irregularities within the TM $\alpha$ bundle, including several kinks induced mostly by Pro residues, a fragment of $3_{10}$ helix in the middle of TM7, and $\alpha$ aneurisms in TM2 and TM5 (*10*). An $\alpha$ aneurism, also referred to as a $\pi$ bulge (*27*), represents a deformation in an $\alpha$ helix caused by the insertion of a single residue (in rhodopsin, these are Gly$^{89}$ and His$^{211}$ in TM2 and TM5, respectively) and is characterized by the formation of two hydrogen bonds of type $i$, $i + 5$ (*28*). However, the observed distortions may not be general structural features of the entire rhodopsin-like family of GPCRs.

For GPCRs, the sequence alignment in TM segments is rather straightforward because of the presence of highly conserved residues in each TM helix and in helix 8; however, an insertion of extra residues in an $\alpha$ helix ($\alpha$ aneurism) can produce a misalignment such as a register shift in an $\alpha$ helix if the target receptor indeed lacks such a helical distortion. To make models suitable for rational ligand design, it is necessary to experimentally validate the accuracy of the proposed models, especially in the area of helical distortions, the less conserved region of the EL2 $\beta$ hairpin, and other loop regions where the sequence alignment is unclear.

Experimental validation can be achieved by the determination of interresidue distances. One method for such determination, the engineering of Zn$^{2+}$-binding sites, has been widely used to study the relative proximity and the dynamics of transmembrane helices in GPCRs (*30–34*). The choice of divalent zinc for the formation of metal-binding sites was based on the lack of redox activity for Zn$^{2+}$, the relatively rapid ligand exchange reaction, and the ability of zinc to interact strongly with a variety of ligand types, including sulfur from cysteine, nitrogen from histidine, and oxygen from glutamate, aspartate, and water (*35*). Each intrinsic and engineered Zn$^{2+}$-binding site provides a set of distances known from the geometry of the tetrahedral sites (*36, 37*), which can be used as constraints for the distance geometry refinement procedure.

In the experiments reported here, we have studied an intrinsic Zn$^{2+}$-binding site of the $\mu$-opioid receptor (MOR) together with newly engineered Zn$^{2+}$-coordination sites between TM5 and TM6 to assess the rhodopsin-based homology model of the MOR in the problematic areas of a $\beta$ hairpin in EL2 and of an $\alpha$ aneurism in TM5. The experimental distance constraints obtained between mutated residues involved in the formation of the metal-binding sites together with distance constraints derived from the rhodopsin structure and the set of $\mu$-specific interhelical hydrogen bonds

between correlated polar residues were used for the modeling of the inactive conformation of the $\mu$ receptor using the distance geometry refinement procedure, as described earlier (*12, 13*).

## EXPERIMENTAL PROCEDURES

*Materials.* The pCMV expression vector containing the coding sequence for the rat MOR was obtained from Professor Huda Akil at the University of Michigan. Pfu turbo DNA polymerase, *Dpn*I restriction endonuclease and XL1-blue super-competent *Escherichia coli* cells were purchased from Stratagene. COS-1 (African green monkey kidney cell line, SV40 transformed) cells were obtained from the American Type Culture Collection (ATCC), CRL-1650. Nucleotide primers, antibiotics, Lipofectamine Plus reagent, cell culture media, and reagents were purchased from Invitrogen. [$^3$H]Naloxone and [$^3$H]DAMGO were purchased from Amersham-Pharmacia and NEN, respectively. The 96-well Multiscreen-FC glass fiber filter plates (MAFCN0B10) were purchased from Millipore. All other reagents were from Sigma−Aldrich unless otherwise indicated.

*Site-Directed Mutagenesis.* Single- and double-point mutations of the rat MOR were generated from the $\mu$/pCMV expression vector using the QuikChange Mutagenesis Kit (Stratagene, La Jolla, CA). Each mutation was verified by DNA cycle sequencing.

*Cell Culture and Transfection.* COS-1 cells were grown to 80% confluency in Dulbecco's modified Eagle's media (high glucose) supplemented with 10% FBS and incubated at 37 °C in 5% CO$_2$. A total of 8 or 10 $\mu$g per 75-cm$^2$ flask of the $\mu$-opioid/pCMV wild-type and mutant plasmids were then transiently transfected into the cells using Lipofectamine Plus reagent (20 and 30 $\mu$L of Plus reagent and Lipofectamine, respectively).

*COS-1 Membrane Preparation.* Whole membrane preparations for radioligand-binding studies were prepared similarly to the established procedures (*38*). Briefly, 48 h after transfection, the COS-1 cells were scraped into 50 mM Tris-HCl at pH 7.4 containing 0.1 mg/mL PMSF (ice-cold) and homogenized using a Polytron homogenizer. After centrifugation at 15000$g$ for 30 min at 4 °C, the membranes were resuspended to a concentration of 0.2 mg/mL in the homogenization buffer. The concentration of membrane protein was determined using the method of Bradford (*39*) with bovine serum albumin as a standard.

*Radioligand-Binding Assays.* The nonspecific opioid antagonist [$^3$H]naloxone and the $\mu$-selective peptide agonist [$^3$H]DAMGO were used for binding studies. For each data point, 40−50 $\mu$g of the COS-1 membrane preparations in 200 $\mu$L of 50 mM Tris-HCl at pH 7.4 were used. The membranes were incubated with 25-$\mu$L aliquots of radioligand in 50 mM Tris-HCl at pH 7.4 in 96-well polypropylene microtiter plates. Radioligand concentrations of 0.1− 20 nM were used for saturation binding studies. Zinc-effect assays were carried out in the presence of 2 nM of radioligand and 0.1 nM−1 mM of ZnCl$_2$. Nonspecific binding was determined in the presence of 2 $\mu$M unlabeled naloxone. After the samples were incubated for 1.5 h at room temperature, they were transferred to 96-well glass fiber filter plates, vacuum filtered, and washed with 2 × 200 $\mu$L of ice-cold 50 mM Tris-HCl at pH 7.4. Filter plates were counted using a Wallac TriLux 1450 scintillation counter.

```
TM1 and IL1
OPSD_BOVIN  34 PWQFSMLAAYMFLLIMLGFPINFLTLYVTVQHKKLRT
OPRM_RAT    65 MVTAITIMALYSIVCVVGLFGNFLVMYVIVRYTKMKT
OPRD_HUMAN  46 LALAIAITALYSAVCAVGLLGNVLVMFGIVRYTKMKT
OPRK_HUMAN  56 PAIPVIITAVYSVVFVVGLVGNSLVMFVIIRYTKMKT
TM2 and EL1
OPSD_BOVIN  71 PLNYILLNLAVADLFMVFGGFTTTLYTSLHGYFVF
OPRM_RAT   102 ATNIYIFNLALADALATS-TLPFQSVNYLMGTWPF
OPRD_HUMAN  83 ATNIYIFNLALADALATS-TLPFQSAKYLMETWPF
OPRK_HUMAN  93 ATNIYIFNLALADALVTT-TMPFQSTVYLMNSWPF
TM3 and IL2
OPSD_BOVIN 106 GPTGCNLEGFFATLGGEIALWSLVVLAIERYVVVCKPMSNRFG-
OPRM_RAT   136 GNILCKIVISIDYYNMFTSIFTLCTMSVDRYIAVCHPVKALDFRT
OPRD_HUMAN 117 GELLCKAVLSIDYYNMFTSIFTLTMMSVDRYIAVCHPVKALDFRT
OPRK_HUMAN 127 GDVLCKIVISIDYYNMFTSIFTLTMMSVDRYIAVCHPVKALDFRT
TM4 and EL2
OPSD_BOVIN 150 ENHAIMGVAFTWVMALACAAPPLV-GWSRYIPEGMQCSCGIDYYTPHEETN
OPRM_RAT   181 PRNAKIVNVCNWILSSAIGLPVMFMATTKYRQG--SIDCTLTFSHPTW-YW
OPRD_HUMAN 162 PAKAKLINICIWVLASGVGVPIMVMAVTRPRDG--AVVCMLQFPSPSW-YW
OPRK_HUMAN 172 PLKAKIINICIWLLSSSVGISAIVLGGTKVREDVDVIECSLQFPDDDYSWW
TM5 and IL3
OPSD_BOVIN 200 NESFVIYMFVVHFIIPLIVIFFCYGQLVFTVKEAAAQQQES
OPRM_RAT   229 ENLLKICVFIFAFIMPVLIITVCYGLMILRLK-SVRMLSGS
OPRD_HUMAN 210 DTVTKICVFLFAFVVPILIITVCYGLMLLRLR-SVRLLSGS
OPRK_HUMAN 223 DLFMKICVFIFAFVIPVLIIIVCYTLMILRLK-SVRLLSGS
TM6 and EL3
OPSD_BOVIN 241 ATTQKAEKEVTRMVIIMVIAFLICWLPYAGVAFYIFTHQ---GSDFG
OPRM_RAT   269 KEKDRNLRRITRMVLVVVAVFIVCWTPIHIYVIIKALITIP-ETTFQ
OPRD_HUMAN 250 KEKDRSLRRITRMVLVVVGAFVVCWAPIHIFVIVWTLVDIDRRDPLV
OPRK_HUMAN 263 REKDRNLRRITRLVLVVVAVFVVCWTPIHIFILVEALGSTS-HSTAA
TM7 and IL4(helix8)
OPSD_BOVIN 285 PIFMTIPAFFAKTSAVYNPVIYIMMNKQFRNCMVTTLCCGKNP
OPRM_RAT   315 TVSWHFCIALGYTNSCLNPVLYAFLDENFKRCFR-EFCIPTSS
OPRD_HUMAN 297 VAALHLCIALGYANSSLNPVLYAFLDENFKRCFR-QLCRKPCG
OPRK_HUMAN 309 LSSYYFCIALGYTNSSLNPILYAFLDENFKRCFR-DFCFPLKM
```

FIGURE 1: Sequence alignment of bovine rhodopsin and the rat $\mu$-, human $\delta$-, and human $\kappa$-opioid receptors. Secondary structure elements were taken from the recent rhodopsin crystal structure (1gzm). The aneurisms are underlined, $\alpha$-helix residues are in bold (purple), and residues in the $\beta$ hairpin of EL2 are in bold italic (green). The row of polar residues from one side of TM2 are shown in blue. The mutated residues participating in the formation of intrinsic and engineered $Zn^{2+}$-binding centers are shown in red.

*Data Analysis.* The saturation-binding results were analyzed, and $K_D$ and $B_{max}$ values for the wild-type (WT) and mutant receptors were determined using the LIGAND module of RADLIG (Biosoft, Ferguson, MO). Saturation-binding experiments were done in duplicate, and values for $K_D$'s were expressed as nanomolars $\pm$ SEM (standard error of the mean). $B_{max}$ values are expressed in picomoles per liter. Competition-binding assays were analyzed using Sigma-maPlot 7.0 (SPSS Science, Chicago, IL). All competition-binding curves were fit by nonlinear regressions, and $IC_{50}$ values were determined from the fitted curve. Average $IC_{50}$ values reported for competition assays are $\pm$ SEM based on two or more independent experiments, each done in duplicate.

*Computational Modeling of MOR.* The procedure includes two major steps: (1) modeling of the MORs using the rhodopsin X-ray structure and (2) distance geometry refinement of the receptor. The MORs were modeled using the recent coordinates of bovine rhodopsin from the Protein Data Bank (code: 1gzm) (*40*) and the alignment of sequences of both proteins from GPCRDB (*19*), slightly modified for the loop regions (Figure 1). The 64 residues from the N terminus were omitted because it has been shown that deletion of these

residues of the MOR has only a minimal affect on the binding of naloxone and DAMGO (*41*). The membrane-bound helix 8 adjacent to TM7 was included in the model, while the rest of the C terminus, conformationally flexible in the rhodopsin structure, was omitted. The side chains of the template were substituted by the residues of the modeled receptors using THREAD, taking the main-chain dihedral angles ($\varphi$ and $\psi$) and the side-chain $\chi^1$ angles from the template. Steric clashes between side chains were removed using alternative side-chain orientations from a rotamer library (*42*). Side chains of polar residues were oriented to maximize the number of mutual hydrogen bonds. The visualization module of QUANTA (MSI) was used for the manual adjustment of the side-chain rotamers to remove major hindrances and to form hydrogen bonds between proximal polar side chains.

Distance geometry calculations of the receptor models were performed with DIANA (*43*), using $C\beta-C\beta$ distances between proximal residues (with an allowed 1 Å deviation) and angle constraints generated from the template, as previously described (*12*, *13*). Interhelical hydrogen bonds between polar side chains of the receptor were obtained from the initial model, validated by several iterative calculations to ensure consistency and added as additional interhelical

Table 1: List of Receptor-Type-Specific Distance Constraints for the Distance Geometry Refinement of the MOR Models

Hydrogen-Bond Distance Constraints (2.9 Å) between Side Chains and between Helices

| proton donors | | proton acceptors | | proton donors | | proton acceptors | |
|---|---|---|---|---|---|---|---|
| residues | atoms | residues | atoms | residues | atoms | residues | atoms |
| Ser[64] | O$\gamma$ | Thr[67] | O$\gamma$1 | Asn[188] | N$\delta$2 | Asn[109] | O$\delta$1 |
| Tyr[75] | O$\eta$ | Gln[124] | O$\epsilon$1 | Asn[191] | N$\delta$2 | Ser[195] | O$\gamma$ |
| Tyr[75] | O$\eta$ | Tyr[128] | O$\eta$ | Trp[192] | N$\epsilon$1 | Asn[109] | O$\delta$1 |
| Asn[86] | N$\delta$1 | Gly[82] | O | Thr[207] | O$\gamma$1 | Tyr[227] | O |
| Asn[86] | N$\delta$2 | Ser[329] | O | Thr[208] | O$\gamma$1 | Tyr[227] | O |
| Asn[86] | N$\delta$2 | Asn[114] | O$\delta$2 | Arg[211] | N$\eta$2 | Ser[222] | O$\gamma$ |
| Arg[95] | N$\eta$2 | Glu[349] | O$\epsilon$2 | Gln[212] | N$\epsilon$2 | Gly[213] | O |
| Tyr[96] | O$\eta$ | Glu[329] | O$\epsilon$1 | Ser[214] | O$\gamma$ | Asp[216] | O$\delta$1 |
| Lys[100] | N$\zeta$ | Ile[93] | O | Ser[214] | O$\gamma$ | His[319] | N$\delta$1 |
| Lys[100] | N$\zeta$ | Tyr[96] | O | Leu[219] | N | Tyr[148] | O$\eta$ |
| Asn[104] | O$\delta$1 | Thr[101] | O$\gamma$1 | Thr[220] | O$\gamma$1 | Lys[209] | O |
| Asn[104] | N$\delta$2 | Tyr[336] | O$\eta$ | His[223] | N$\delta$1 | Phe[221] | O |
| Tyr[106] | O$\eta$ | Asn[183] | O$\delta$1 | His[223] | N$\epsilon$2 | Glu[310] | O$\epsilon$1 |
| Asn[109] | N$\delta$2 | Asn[191] | O$\delta$1 | Asn[230] | N$\delta$2 | Thr[307] | O$\gamma$1 |
| Asn[109] | N$\delta$2 | Thr[157] | O$\gamma$1 | Lys[233] | N$\zeta$ | Glu[229] | O$\epsilon$1 |
| Thr[118] | O$\gamma$1 | Gly[82] | O | Arg[258] | N$\epsilon$ | Arg[258] | O |
| Thr[120] | O$\gamma$1 | Ile[142] | O | Arg[258] | N$\eta$1 | Ser[261] | O$\gamma$ |
| Gln[124] | N$\epsilon$2 | Ile[215] | O | Arg[258] | N$\eta$2 | Asp[272] | O$\delta$2 |
| Gln[124] | O$\epsilon$1 | Tyr[326] | O$\eta$ | Arg[273] | N$\epsilon$ | Ser[268] | O$\gamma$ |
| Asn[127] | N$\delta$2 | Ser[214] | O | Trp[293] | N$\epsilon$1 | Asn[328] | O$\delta$1 |
| Thr[132] | N | Asn[127] | O$\delta$1 | Thr[307] | O$\gamma$1 | Glu[229] | O$\epsilon$1 |
| Trp[133] | N$\epsilon$1 | Gln[215] | O$\epsilon$1 | Thr[315] | O$\gamma$1 | Asp[216] | O$\delta$2 |
| Trp[133] | N$\epsilon$1 | Ile[215] | O | Trp[318] | N$\epsilon$1 | Thr[218] | O$\gamma$1 |
| Asn[137] | N$\delta$2 | Tyr[210] | O | His[319] | N$\epsilon$2 | Tyr[128] | O$\eta$ |
| Lys[141] | N$\epsilon$ | Met[203] | O | His[319] | N$\delta$1 | Asp[216] | O$\delta$2 |
| Tyr[149] | O$\eta$ | Ser[196] | O$\gamma$ | His[319] | N$\delta$1 | Asp[216] | O$\delta$1 |
| Asn[150] | N$\delta$2 | Asp[114] | O$\delta$1 | Tyr[326] | O$\eta$ | Asp[147] | O$\delta$2 |
| Thr[153] | O$\gamma$1 | Ser[195] | O$\gamma$ | Asn[328] | N$\delta$2 | Asn[150] | O$\delta$1 |
| Thr[157] | O$\gamma$1 | Asn[191] | O$\delta$1 | Asn[332] | N$\delta$2 | Asp[114] | O$\delta$1 |
| Arg[165] | N$\eta$2 | Asp[164] | O$\delta$1 | Asn[332] | N$\delta$2 | Ser[154] | O$\gamma$ |
| Arg[165] | N$\epsilon$ | Thr[279] | O$\gamma$1 | Asn[332] | N$\delta$2 | Asn[328] | O |
| Arg[165] | N$\eta$1 | Thr[279] | O$\gamma$1 | Lys[344] | N$\epsilon$ | Phe[338] | O |

| residues | atoms | residues | atoms | distances (Å) |
|---|---|---|---|---|
| | | **Disulfide Bond Constraints** | | |
| Cys[140] | C$\beta$ | Cys[217] | C$\beta$ | 4.20 |
| Cys[140] | C$\beta$ | Cys[217] | S$\gamma$ | 3.05 |
| Cys[140] | S$\gamma$ | Cys[217] | G$\beta$ | 3.05 |
| Cys[140] | S$\gamma$ | Cys[217] | S$\gamma$ | 2.04 |
| | | **Zn$^{2+}$-Binding Site Constraints for "Mutant" Receptor Model** | | |
| Cys[234] | S$\gamma$ | Cys[237] | S$\gamma$ | 3.90 |
| Cys[234] | C$\beta$ | His[297] | C$\beta$ | 8.50 |
| Cys[234] | C$\beta$ | Cys[300] | C$\beta$ | 7.50 |
| Cys[234] | S$\gamma$ | His[297] | N$\epsilon$2 | 3.50 |
| Cys[234] | S$\gamma$ | Cys[300] | S$\gamma$ | 3.50 |
| Cys[237] | C$\beta$ | His[297] | C$\beta$ | 6.50 |
| Cys[237] | S$\gamma$ | His[297] | N$\epsilon$2 | 3.40 |
| Cys[237] | C$\beta$ | Cys[300] | C$\beta$ | 6.50 |
| Cys[237] | S$\gamma$ | Cys[300] | S$\gamma$ | 3.80 |
| Cys[300] | S$\gamma$ | His[297] | N$\epsilon$2 | 3.20 |

distance constraints (Table 1). In calculations with DIANA, the angles and the hydrogen-bond distance constraints appropriate for $\alpha$ helices ($\varphi = -70$ to $-50°$, $\psi = -50$ to $-30°$, upper limit for NH$_i$···O$_{i-4}$ distance is 1.9 Å) and for $\beta$ sheet ($\varphi = -150$ to $-90°$, $\psi = +90$ to $+150°$) were used, except in the case of Pro kinks and $\alpha$ aneurisms. The standard target function minimization strategy (43) was used for the calculations. The target (scoring) function represents the sum of weighted violations of distance (upper and low) and dihedral constraints and the penalty for possible overlaps between contacting atoms. Several variants of loop-residue alignments with rhodopsin (1gzm) were tested during distance geometry refinement for consistency with other distance and angle constraints. The final structure with the lowest target function corresponded to the alignment pre-

sented in Figure 1, where an extra residue was added at the end of TM4, two residues were deleted from the turn of the $\beta$ hairpin, one from the end of EL2, one from the end of TM5, and one from helix8, one residue was added at the end of intracellular loop 2 (IL2), and three extra residues in EL3 formed a turn of the $\alpha$ helix. In the calculated structure, the end of EL2 adjacent to TM5 was flexible, demonstrating several conformations that were different from the rhodopsin structures.

During the refinement procedure, the $\alpha$ aneurism present in the rhodopsin template was removed from TM2 based on the following evidence. First, all sequences of opioid receptors are one residue shorter than the rhodopsin sequence in this part of TM2, suggesting that the extra-residue insertion is unlikely in the opioid receptors. Second, all opioid
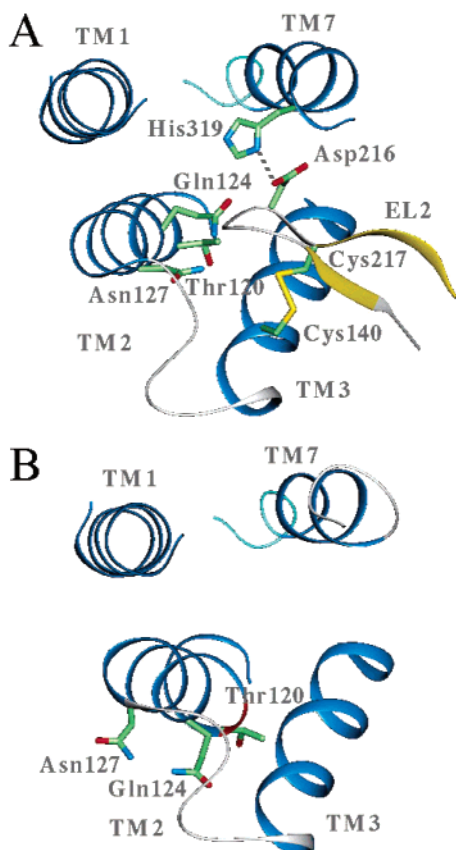
FIGURE 2: Extracellular part of TM1, TM2, TM3, and TM7 of the rat MOR. (A) Refined model with the $\beta$ hairpin (EL2) connected to TM3 by a disulfide bond between Cys[140] and Cys[217] and to TM7 by an intrinsic $Zn^{2+}$-binding site formed by Asp[216] and His[319]. Exclusion of the $\alpha$ aneurism from TM2 allows the polar residues Thr[120], Gln[124], and Asn[127] to face the ligand-binding cleft. (B) Unrefined model with an $\alpha$ aneurism in TM2, similar to the rhodopsin template, where the polar residues Thr[120], Gln[124], and Asn[127] face the lipid bilayer.

receptors have a row of polar residues located in $i$, $i + 4$, and $i + 7$ positions along one side of the $\alpha$ helix in TM2 (Thr[120], Gln[124], and Asn[127] in the $\mu$ receptor, the corresponding Thr[101], Gln[105], and Lys[108] of the $\delta$ receptor, and Thr[111], Gln[115], and Val[118] of the $\kappa$ receptor). This row of polar residues is oriented toward the ligand-binding pocket if TM2 has ideal $\alpha$ helix geometry, as illustrated in Figure 2A but faces the membrane lipid if an $\alpha$ aneurism is retained in TM2 (Figure 2B). Indeed, Asn[127] of the $\mu$ receptor and the corresponding Lys[108] in the $\delta$ receptor have been shown to be important for ligand binding (44). These observations suggest that these polar residues in TM2 of $\mu$- and $\delta$-opioid receptors are oriented toward the ligand-binding pocket and indicate the absence of an $\alpha$ aneurism in TM2. Recently published $\delta$-opioid receptor models (20, 21) and the automatically generated models of other opioid receptors (19) retain the $\alpha$ aneurism found in TM2 of rhodopsin, resulting in the unlikely reorientation of a polar cluster toward the lipid bilayer (Figure 2B). Our alignment also differs from the one proposed in these models, near the helix ends, helix distortions, and in the loop regions. The presence or absence of distortions in TM2 appear to be receptor-specific and therefore require experimental verification. For example, cysteine-scanning mutagenesis data are consistent with the presence of an $\alpha$ aneurism in TM2 of the dopamine D2

receptor (45), while the pattern of polar residues in TM2 of melanocortin receptors and their involvement in ligand binding (46, 47) indicate the absence of an $\alpha$ aneurism in TM2 of these receptors.

Four sets of distance constraints were used for calculation of MOR models with two different geometries of TM5 (Table 2): one similar to the rhodopsin structure with an $\alpha$ aneurism at Ala[240] (type-1 model) and another without the $\alpha$ aneurism (type-2 model). The reference type-1 model with rhodopsin-like geometry of TM5 was calculated without the additional constraints derived from the incorporation of a metal-binding site between TM5 and TM6. In the other three sets of models, the additional distance constraints between TM5 and TM6 were included in calculations, consistent with the tetrahedral geometry of $Zn^{2+}$-binding centers (36): 6.5−8.5 Å distances between $C\beta−C\beta$ atoms and 3.2−4.0 Å distance constraints between O, N, and S atoms of the residues participating in the formation of $Zn^{2+}$-binding sites (Table 3). During calculations the side chains of residues in positions 234, 237, and 300 were retained, such as in the native sequence of the MOR, or replaced by cysteines, such as in the engineered mutants. In all approximations, EL2 was taken from the rhodopsin template (see alignment in Figure 1), as a $\beta$ hairpin with S−S bond between Cys[140] and Cys[217] (48) and with Asp[216] forming an intrinsic $Zn^{2+}$-binding center with His[319] from TM7, consistent with the experimental observations described below.

For each distance geometry calculation, the five best structures with the lowest target functions were analyzed. The selection of the best receptor model among several alternatives was assisted by docking opioid ligands and examining which model(s) provided the best, most consistent fit. Ligand docking was performed manually using QUANTA modules, followed by the DOCK application incorporated in QUANTA. Docking was performed in a stepwise manner using a set of opioid ligands. The first docking candidate was the large rigid alkaloid norBNI, which binds to the MOR with relatively high affinity ($K_D \sim 10$ nM). This was followed by naloxone, used in the binding assay. The docking was directed by proposed electrostatic interactions between the $N^+$ of the ligands and the conserved Asp[147] in TM3 of the $\mu$ receptors, by hydrogen-bond formation between the OH group of the ligand tyramine moiety and the conserved His[297] in TM6, and by the proximity between the second $N^+$ of norBNI and Lys[303] in TM6, a position occupied by Glu[297] in the $\kappa$-opioid receptor, an important residue for the increased norBNI-binding affinity to the $\kappa$ receptor (49). The atomic coordinates of the refined model of the rat MOR (inactive state) with norBNI bound have been deposited on our web site (http://mosberglab.phar.umich.edu/resources/index.php).

## RESULTS

*An Intrinsic $Zn^{2+}$-Binding Center in the MOR Is Formed by His[319] and Asp[216].* The zinc sensitivity of the WT receptor and receptor mutants was evidenced by reduced radioligand ligand binding in the presence of increasing amounts of $ZnCl_2$. The affinities of the intrinsic and engineered $Zn^{2+}$-binding sites were assayed by inhibition of [$^3$H]naloxone or [$^3$H]DAMGO binding and the $IC_{50}$ values for $Zn^{2+}$ inhibition (the concentration of $ZnCl_2$ that disrupted 50% of radioligand

Table 2: RMSD between Distance Geometry Refined Models of Rat MOR (Model with the Best Target Function) and the Rhodopsin Template[a]

| models | α aneurism in TM5 | TM5−TM6 constraints | residues 234, 237, and 300 | RMSD (Å) | | | target function |
| | | | | within model set[b] | versus TM of rhodopsin[c] | versus TM5−TM6 of rhodopsin[d] | |
|---|---|---|---|---|---|---|---|
| reference | + | − | native | 0.50 ± 0.09 | 1.07 | 1.31 | 49.3 |
| type-1 native | + | + | native | 0.67 ± 0.07 | 1.22 | 1.44 | 54.7 |
| type-1 mutant | + | + | cysteines | 0.69 ± 0.08 | 1.18 | 1.44 | 51.7 |
| type-2 native | − | + | native | 0.63 ± 0.06 | 1.17 | 1.38 | 67.7 |

[a] Sets of calculated models differ by the presence or absence of an α aneurism in TM5, by the substitutions for residues in positions 234, 237, and 300 for cysteine, and by the incorporation of additional distance constraints between TM5 and TM6 appropriate for the zinc-binding sites. [b] For all 291 Cα atoms, the pairwise superposition of four structures with the best model. [c] For 235 Cα atoms of TM fragments, helix 8, and β hairpin. [d] For 59 Cα atoms of TM5 and TM6.

Table 3: Endogenous and Artificially Created Zinc-Binding Centers in the MOR: Effect of Zn$^{2+}$ on the Binding of the Radioligand[a]

| mutants | [$^3$H]naloxone | | [$^3$H]DAMGO | |
| | $K_D$ (nM) | Zn$^{2+}$ IC$_{50}$ ($\mu$M) | $K_D$ (nM) | Zn$^{2+}$ IC$_{50}$ ($\mu$M) |
|---|---|---|---|---|
| $\mu$ WT | 1.8 ± 0.3 | 32.6 ± 3.7 (3) | 1.1 ± 0.33 | 62.2 ± 3.8 (4) |
| H297Q | nb[b] | nb | 0.96 ± 0.25 | 61.0 ± 4.0 (2) |
| H319N | 5.0 ± 2.0 | 200.0 ± 22.0 (2) | nb | nb |
| H223N/H319N | 4.0 ± 2.0 | 300.0 ± 30.0 (2) | nb | nb |
| D216V | 3.6 ± 1.4 | 70.0 ± 5.7(3) | 0.9 ± 0.6 | 175.0 ± 9.3 (3) |
| N230H | 1.2 ± 0.2 | 32.5 ± 2.5 (2) | 1.0 ± 0.11 | 41.7 ± 6.0 (3) |
| I234C | 1.4 ± 0.3 | 32.5 ± 2.5 (2) | 1.3 ± 0.12 | 40.0 ± 5.6 (2) |
| F237H | 2.8 ± 1.6 | 25.0 ± 3.0 (2) | 3.5 ± 1.7 | 10.0 ± 1.1 (3) |
| V300C | 1.3 ± 0.2 | 20.0 ± 1.6 (3) | 2.5 ± 0.89 | 21.0 ± 1.4 (3) |
| N230H/I234C | 1.4 ± 0.7 | 32.0 ± 1.7 (3) | 0.58 ± 0.06 | 16.0 ± 0.9 (3) |
| I234C/V300C | 2.6 ± 1.4 | 6.7 ± 0.25 (3) | 0.97 ± 0.40 | 16.6 ± 1.6 (3) |
| I234C/F237C | 2.6 ± 1.7 | 3.0 ± 0.17 (4) | 0.84 ± 0.17 | 6.2 ± 0.42 (3) |
| F237C/V300C | 3.8 ± 2.7 | 10.0 ± 1.4 (3) | 3.7 ± 1.8 | 16.6 ± 2.9 (3) |
| F237C/F241H | 5.0 ± 2.8 | 45.0 ± 3.7 (4) | 0.94 ± 0.2 | 16.4 ± 2.2 (3) |
| I234C/F237C/H297Q | nb | nb | 5.7 ± 1.3 | 50.0 ± 6.0 (4) |
| I234C/F237C/H319N | 6.4 ± 0.5 | 30.0 ± 2.4 (2) | nb | nb |

[a] Competition assays were carried out in the presence of 2 nM [$^3$H]naloxone and 0.1 $\mu$M−1000 mM ZnCl$_2$. Nonspecific binding was determined in the presence of 2 mM unlabeled naloxone. Values reported are ± SEM based on two or more independent experiments (number in parentheses), each done in duplicate. [b] nb = no displaceable, specific ligand binding observed.

binding) in the WT and in the mutants of the rat MORs are summarized in Table 3.

Although the $\kappa$- and $\delta$-opioid receptors have been reported to be relatively insensitive to Zn$^{2+}$ (33, 50), our results demonstrate that Zn$^{2+}$ significantly reduces naloxone and DAMGO binding to the WT $\mu$ receptor with IC$_{50}$ = 32.6 ± 3.7 and 62.2 ± 3.8 $\mu$M, respectively. To determine whether any of the histidine residues present in the extracellular half of the MOR contribute to this intrinsic, relatively high-affinity Zn$^{2+}$-binding center, we examined the effect of the replacement of each of three histidines from TM6 (His$^{297}$), TM7 (His$^{319}$), and EL2 (His$^{223}$) by residues incapable of chelating Zn$^{2+}$. The corresponding mutants were H297Q, H319N, and the H223N/H319N double mutants. The double mutant was designed to verify the possible interaction between residues His$^{223}$, located in EL2, and His$^{319}$, in TM7, which are distant in the rhodopsin-based model (C$\beta$−C$\beta$ distance ∼ 19 Å) but can approach each other if EL2 exhibits rather high flexibility.

Differential effects on agonist and antagonist binding have been reported for mutations of H297 and H319 in the $\mu$ receptor. It has been reported that H297N substitution does not affect DAMGO binding but decreases naloxone binding (51). In contrast, naloxone affinity for the H319A $\mu$-receptor mutant is similar to that for the $\mu$ WT, while DAMGO affinity is greatly reduced (52). As shown in Table 3, our results for the H297Q, H319N, and H223N/H319N mutants

are consistent with these following observations: the H297Q mutant loses the ability to bind naloxone, but binding of DAMGO is unaffected, while the H319N and H223N/H319N mutants bind naloxone with high affinity but do not bind DAMGO.

It can be seen from Table 3 that the H297Q mutation has no effect on the Zn$^{2+}$ sensitivity of DAMGO binding, an indication that His$^{297}$ does not participate in the intrinsic Zn$^{2+}$-binding site of the WT receptor. In contrast, replacing His$^{319}$ in both the H319N single and H223N/H319N double mutant greatly reduced sensitivity of naloxone binding to Zn$^{2+}$ (IC$_{50}$ values of 200 and 300 $\mu$M, respectively). These results indicate that His$^{319}$ is the most likely coordination site for Zn$^{2+}$ in the native $\mu$ receptor, while other extracellular histidines are not involved in Zn$^{2+}$ binding. Moreover, His$^{223}$ remains distant from His$^{319}$, as in the rhodopsin X-ray structure. It is thus likely that one or more EL2 or TM3 Asp, Glu, or Cys residues proximal to His$^{319}$ also contributes to the Zn$^{2+}$ binding of the WT receptor.

Recent cysteine-scanning mutagenesis of the dopamine D2 receptor confirmed that EL2 of this rhodopsin-like GPCR preserves a $\beta$-hairpin-like conformation similar to rhodopsin (53). We suggest that EL2 in the $\mu$ receptor can also retain this $\beta$-hairpin-like structure with deletion of two residues from the turn region (see alignment in Figure 1). In this EL2 conformation, Asp$^{216}$ would be near His$^{319}$ and thus could participate, along with His$^{319}$, in the endogenous Zn$^{2+}$-

binding site. Indeed, the mutation of Asp[216] to Val, the corresponding residue in the $\delta$ receptor, decreases the inhibitory effect of $Zn^{2+}$ on both naloxone and DAMGO binding (Table 3). These data suggest that residues His[319] and Asp[216] of the $\mu$ receptor are, in fact, close to each other and participate in the formation of the intrinsic $Zn^{2+}$-binding site. In any rhodopsin-like model of the $\mu$ receptor, no other aspartate, glutamate, or cysteine residues are in the vicinity of His[319]. The closest such residue, Asp[147] from TM3, is rather distant from His[319] (C$\beta$–C$\beta$ distance $\sim$ 13 Å) and therefore is unlikely to be involved in $Zn^{2+}$ coordination.

*An Engineered High-Affinity $Zn^{2+}$-Binding Site Is Formed by Residues I234C, F237C, and V300C and His[297] of TM5 and TM6.* To test the relative position of the flexible TM5 and TM6 and to assess the structural features of the region of possible distortion in TM5 of the MOR near Ala[240] (corresponding to the $\alpha$ aneurism in rhodopsin), we mutated residues near Ala[240] in TM5 and TM6 to either Cys or His (depending upon which replacement introduced the least distortion of the helices in our molecular model) to facilitate possible $Zn^{2+}$ binding, taking advantage, too, of the proximal native His[297] of TM6. The residues chosen for mutation (Phe[237], Phe[241], and Val[300]) lie 2–4 helical turns from the extracellular ends of TM5 and TM6. We also mutated residue Ile[234] in the second turn of TM5, which faces the lipid environment in the rhodopsin-like structure but would be reoriented toward the binding-site crevice in the absence of an $\alpha$ aneurism. By comparing the relative zinc affinities of mutants of various residues up and down TM5 and TM6, we were able to deduce the relative position of these two helices and the proximities of their residue side chains. Then, if a receptor mutant exhibits a lower $IC_{50}$ for $Zn^{2+}$ binding than the WT, the mutated residues are considered to be in close proximity to the native His[297]. Evidence in support of the role of His[297] is described below.

In the absence of $Zn^{2+}$, most mutant receptors studied bound the nonselective antagonist naloxone and the $\mu$-selective peptide agonist DAMGO with $K_D$ values similar to that of the WT, indicating that the opioid-binding pocket was well-preserved in these mutants. Notable exceptions are the H297Q and I234C/F237C/H297Q mutants, which lose the capacity to bind naloxone, and the I234C/F237C/H319N mutant with no binding of DAMGO. For the single-residue mutations of the TM5 and TM6 residues, the effect on $Zn^{2+}$ binding is generally small. However, introduction of a Cys residue in place of Val[300], located one turn from His[297] in TM6, decreases the $Zn^{2+}$ $IC_{50}$ for DAMGO binding by $\sim$3-fold, while incorporation of His in TM5 in place of Phe[237], opposite His[297] of TM6, ($\sim$8-Å C$\beta$–C$\beta$ distance in the rhodopsin structure) decreases $Zn^{2+}$ $IC_{50}$ for DAMGO by $\sim$6-fold. The $Zn^{2+}$ sensitivity of naloxone binding was also increased for the V300C mutant but to a lesser extent. Notably, the incorporation of a single His or Cys residues in place of Asn[230] or Ile[234], both more distant from His[297] (C$\beta$–C$\beta$ distance of 17.8 and 13.9 Å, respectively, in the rhodopsin structure), does not change $Zn^{2+}$ sensitivity of naloxone binding.

A similar tendency is observed for the double mutants. As can be seen in Table 3, the N230H/I234C double mutant shows no enhancement of $Zn^{2+}$ sensitivity of the naloxone binding relative to that of the WT. On the other hand, the F237C/V300C double mutant demonstrates increased $Zn^{2+}$

sensitivity of naloxone binding ($IC_{50} \sim 10\mu M$) relative to that of the WT and to the corresponding single mutants. These observations correlate with the relative locations of Asn[230], Ile[234], Phe[237], and Val[300] from His[297]. While the first residue pair is distant from His[297], the second pair is proximal to His[297] and could form a tridentate metal-binding site. The results for the F237C/F241H mutant are less clear because of reduced naloxone binding in the absence of $Zn^{2+}$.

The results for the I234C/V300C and I234C/F237C double mutants, in which a cysteine residue is incorporated into the Ile[234] position, located on the lipid-exposed face of TM5 in the rhodopsin template, are particularly interesting. As seen in Table 3, the I234C/V300C double mutant shows an approximately 5-fold enhancement, while I234C/F237C shows a 10-fold enhancement of the sensitivity to $Zn^{2+}$ for both naloxone and DAMGO binding, suggesting that, in each case, both mutated residues, along with His[297], participate in forming the $Zn^{2+}$-binding center. It should be pointed out that the nominal 5–10-fold increase in $Zn^{2+}$ sensitivity is a considerable underestimate, because the effect is masked by the presence of the intrinsic $Zn^{2+}$-binding site. The participation of His[297], assumed in the design of the experiments, is confirmed by the lack of $Zn^{2+}$ sensitivity for DAMGO binding displayed by the triple mutant I234C/F237C/H297Q. The involvement of Ile[234] in $Zn^{2+}$ binding indicates that Ile[234] is oriented away from the lipid environment in the MOR and toward the ligand-binding crevice, in direct contradiction of the prediction from the rhodopsin-based model.

*Refinement of the Homology Model of the MOR Using Experimental Distance Constraints.* The data obtained that indicate proximity between residues His[319] (TM7) and Asp[216] (EL2), which participate in an intrinsic zinc-binding center, and between Phe[237] (TM5) and Val[300] or His[297] (TM6), inferred from the engineered metal-binding center, agree with the observed distances of 7–9 Å between C$\beta$–C$\beta$ atoms of the corresponding residues in the rhodopsin template. However, the experimentally observed involvement of I234C in the artificially designed metal-binding center between TM5 and TM6 is inconsistent with the rhodopsin template, which places Ile[234] in the lipid environment away from the ligand-binding crevice and where C$\beta$–C$\beta$ distances between Ile[234] and His[297] and between Ile[234] and Val[300] (13.9 and 12.9 Å, respectively) are too large to allow participation in the same $Zn^{2+}$-binding site. However, Ile[234] can be oriented toward the ligand-binding pocket and could approach residues Val[300] and His[297] in TM6 if the $\mu$ receptor lacks an $\alpha$ aneurism at Ala[240] or if there is an increased kink angle at Pro[244], allowing the extracellular part of TM5 to bend toward TM6.

To choose between these possibilities and to assess the likelihood of the $\alpha$ aneurism in TM5 of the MOR, the homology model of the inactive MOR was refined by distance geometry calculations as described in the Experimental Procedures.

Four sets of models with (type 1) and without (type 2) an $\alpha$ aneurism in TM5 and with and without the structural restraints between positions 234–237–297–300 derived from the $Zn^{2+}$-binding studies described above were calculated (Table 2). All types of models superimpose well with the C$\alpha$ atoms of the corresponding residues of the rhodopsin structure (using the alignment in Figure 1) with RMSD $\sim$ 1.2 Å for 215 C$\alpha$ atoms in TM helices, helix 8, and the $\beta$ hairpin in EL2 and with RMSD = 1.6–1.8 Å for all 263
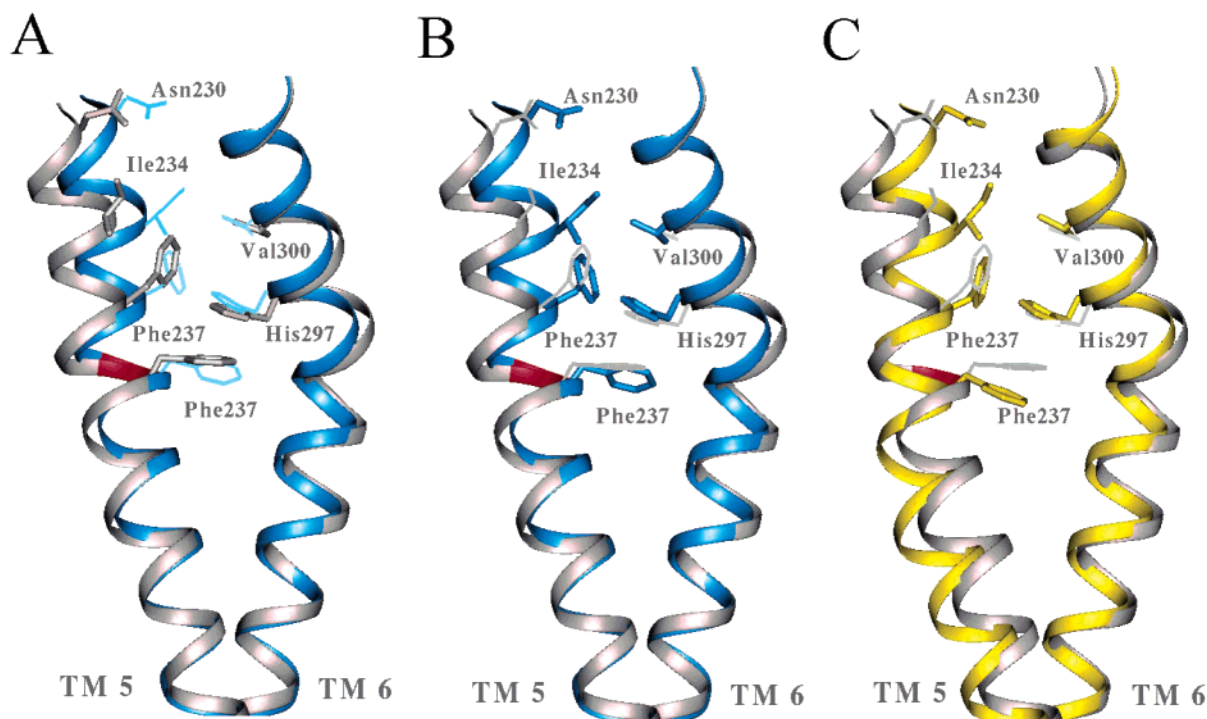
FIGURE 3: Comparison of the refined models of rat MOR. (A and B) Superposition of TM5 and TM6 of the type-1 models. Reference model (gray color; the Cβ−Cβ distances between residues 234 and 297 and between residues 234 and 300 are 13 and 12.4 Å, respectively) and refined model calculated with restraints between residues 234−237−297−300, corresponding to the formation of the Zn²⁺-binding site (blue color; the Cβ−Cβ distances between residues 234 and 297 and between residues 234 and 300 are 9 and 7.5 Å, respectively). (C) Superposition of TM5 and TM6 of the type-1 reference model (gray color) and the type-2 model, calculated without α aneurism in TM5 and with restraints between residues 234−237−297−300 (yellow color). The α aneurism at Ala²⁴⁰ is indicated in red.

corresponding Cα atoms. The reference rhodopsin-like models, calculated without the additional Zn²⁺-binding restraints, had the lowest RMSD ∼ 1.1 Å, compared to the rhodopsin template. The pairwise RMSD for each helix of the best reference structure are 0.87 (TM1, 31 atoms), 1.03 (TM2, 29 atoms), 0.75 (TM3, 33 atoms), 1.05 (TM4, 24 atoms), 1.27 (TM5, 28 atoms), 1.34 (TM6, 31 atoms), and 1.10 Å (TM7, 24 atoms), respectively, and have ∼2-Å shifts in the extracellular parts of TM2, TM4−6, and the intracellular part of TM7, with larger shifts in the loop regions. Alternative conformations of the less-constrained region 220−227 in EL2 were obtained for different suboptimal structures. During calculations, the α aneurism was removed from TM2 (see the Experimental Procedures), which brought the polar residues Gln¹²⁴ and Asn¹²⁷ inside the TM α bundle, where they participate in the network of hydrogen bonds with Tyr⁷⁵ (TM1), Tyr¹²⁸ (TM2), Tyr³²⁶ (TM7), and the backbone of EL1 and EL2 (Table 2). Interestingly, for the models calculated with TM5−TM6 Zn²⁺-coordination restraints, the type-1 models were closer to the rhodopsin structure in the intracellular half of TM5, while the extracellular end of TM5 was shifted toward TM6 because of the concerted adjustments of the backbone angles in the region 211−241 and an increased kink near Pro²⁴⁴ to satisfy the additional constraints (Figure 3). Moreover, the target functions of the 5 best models of type 1 were 45−59 as compared to the target functions of 54−70 for the 5 best models of type 2, because of better side-chain packing between TM3 and the intracellular half of TM5. In the models of type 2, the entire TM5 was slightly shifted and the interactions between residues of TM3 and the intracellular part of TM5 were changed, causing the observed increase of the target function

because of steric hindrances. Thus, the type-1 models, which retain the α aneurism in TM5, provided fewer hindrances and better consistency for all structural restraints.

## DISCUSSION

To test the model of the MOR, we utilized the zinc-binding site engineering method applied earlier for GPCRs (*30−34*). However, we observed that in the WT MOR Zn²⁺ significantly inhibited naloxone and DAMGO binding with IC₅₀ values of 32.6 ± 3.7 and 62.2 ± 3.8 μM, respectively. These experiments confirmed the early observations that micromolar concentrations of Zn²⁺ affected ligand binding for the MOR, while δ and κ receptors were insensitive to Zn²⁺ (*50, 54*). The micromolar affinity of the WT μ receptor to Zn²⁺ may indicate the presence of at least a bidentate endogenous Zn²⁺-coordination site likely formed by histidine, cysteine, aspartate, or glutamate residues (*37*).

Recently, allosteric Zn²⁺-binding sites have been demonstrated in different GPCRs. For example, the enhancing effect of Zn²⁺ to β-adrenoreceptor activation was associated with a high-affinity site (IC₅₀ ∼ 5 μM) formed by His²⁶⁹, Cys²⁶⁵, and Glu²²⁵ from the intracellular ends of TM6 and TM5 (*55*). On the other hand, the observed stimulatory effects of micromolar Zn²⁺ on the activation of the melanocortin MC1 receptor has been related to residues from the extracellular part of the receptor: Cys²⁷¹ from EL3 and Asp¹¹⁹ from the extracellular end of TM3 (*56, 57*). The positive modulator effect of Zn²⁺ on tachykinin NK3 receptor activation was also attributed to the extracellular residues His²⁴⁴ and His²⁴⁸ from the end of TM5 (*58*). Analogously, the intrinsic Zn²⁺-binding site in the MOR may negatively regulate the receptor

activity through the inhibition of the binding of the agonist and antagonists.

Our data indicate that in the MOR an intrinsic metal-binding center is formed by at least His[319] from TM7 and Asp[216] from EL2. Other opioid receptors are insensitive to $Zn^{2+}$, possibly because they do not have both of these residues in the $\delta$ and $\kappa$ receptors; the corresponding residues are His[301]-Val[197] and Tyr[313]-Glu[208], respectively. In the $\mu$ receptor, Asp[216] is located in EL2, which can form a $\beta$ hairpin inserted between the TM helices and attached by a disulfide bond to TM3, as in the rhodopsin structure. In our previous models of the opioid receptors, we proposed a $\beta$-hairpin-like structure for EL2 of all opioid receptors based on the analysis of the side-chain propensities and the polarity pattern of the residues in the loops (*13*). Indeed, in the $\mu$-receptor model based on the rhodopsin template (see alignment in Figure 1), Asp[216] is located in the turn of the $\beta$ hairpin that is close to His[319] from TM7, enabling the formation of a zinc-binding site between these two residues (Figure 2), consistent with our experimental observations. Thus, the rhodopsin crystal structure can be regarded as a suitable template for the modeling not only of the seven TM $\alpha$ bundle, but also of EL2 of the MOR.

To assess whether an $\alpha$ aneurism exists in TM5 of the MOR and to investigate the interface between TM5 and TM6, we utilized the zinc-binding site engineering method. This method has been adapted for determining the proximity of residues in a number of GPCRs, including residues in several helices of the tachykinin NK$_1$ receptors (*30–32*), the $\kappa$-opioid receptors (*33*), rhodopsin (*59*), the $\beta$-adrenergic receptor, and the parathyroid-hormone receptor (*60*). More recently, metal-binding sites enhancing G protein activation have been artificially created between TM3 and TM7 of the $\beta$2-adrenergic (*34*) and the tachykinin NK$_1$ receptors (*32*) and between TM2 and TM3 of the MC4 melanocortin receptor (*61*). Moreover, proximity between TM5 and TM6 has been previously studied in NK$_1$ and $\kappa$-opioid receptors by engineering a $Zn^{2+}$-binding site at the juncture of EL2 and EL3 (*30, 33*). The published data on engineered metal-binding sites between TM5 and TM6 (*30, 33*) correlate well with the observed distances of 5.2–9.2 Å between C$\beta$ atoms of the corresponding residues in the rhodopsin structure. However, these data do not provide information that allows a reliable conclusion about the presence or absence of the $\alpha$ aneurism in the middle of TM5, because the mutated residues in these studies are located near the extracellular end of TM5, while the $\alpha$ aneurism is fairly remote, in the fourth turn of TM5. To investigate the possible TM5 distortion in the $\mu$ receptor, we elected to study the proximity between residues of TM5 and TM6 located closer to the middle of the helix, in helical turns 2–4, making use of the naturally present His[297] in the third helical turn of TM6. The observation that the designed double mutants Ile234C/Phe237C and Ile237C/Val300C demonstrate ~5–10-fold enhancement of the $Zn^{2+}$ sensitivity relative to the WT $\mu$ receptor (Table 2) indicates the formation of high-affinity artificial metal-binding sites between His[297] and cysteines substituted for Ile[234], Phe[237], and Val[300] in the mutant $\mu$ receptors. The geometry of the $Zn^{2+}$-binding site, formed by two cysteines and one histidine from TM5 and TM6, can then be used to refine the position of these structurally flexible helices and to verify the presence of the $\alpha$ aneurism at Ala[240] by distance geometry calculations.

Our calculations allowed the refinement of a comparative model of the MOR based on the rhodopsin crystal structure to remove hindrances between $\mu$-specific side chains and to satisfy the hydrogen-bonding potential of interhelical polar residues of the $\mu$ receptor. The calculations confirm that an $\alpha$ aneurism is absent from TM2 but is likely to be present in TM5 of the opioid receptors. Further, the calculations indicate that EL2 has a $\beta$-hairpin-like structure and is inserted between the TM helices, attached to TM3 by a Cys[140]-Cys[217] disulfide bond and to TM7 by a $Zn^{2+}$-coordination site formed by His[319]-Asp[216]. Moreover, the extracellular part of TM5 appears to be highly flexible, possibly because of the presence of the $\alpha$ aneurism at Ala[240] and the Pro[244]-induced kink, which facilitate a shift of TM5 toward TM6, to adjust the shape of the ligand-binding pocket. Previous observations have also indicated high structural flexibility of TM5 as judged from the higher *B* factor for this helix in the rhodopsin structure (*62*) and the broad pattern of accessibility observed for 10 consecutive residues in the extracellular part of TM5 of the dopamine receptor (*63*). Similar helical motion could be expected for TM6 near the binding pocket because of the presence of the conserved Pro[295]. Indeed in the $\mu$-, $\delta$-, and $\kappa$-opioid receptors, a wide area of accessibility was recently demonstrated for the extracellular side of TM6 (*64*).

The implication of the studies presented here is clear: the rhodopsin X-ray structure is a suitable template for the modeling of other GPCRs, but it should be used with caution for the homology modeling of receptors with low sequence identity to rhodopsin, a category that includes most members within the rhodopsin family. To improve accuracy, the calculated models of each particular receptor should be verified experimentally, as in the example presented here, especially for regions where distortions occur and for areas of low homology where structural differences can be expected. The described experimental verification of the MOR model using experimental constraints derived from the intrinsic and the artificially designed $Zn^{2+}$-binding sites in the MOR shows that the rhodopsin template may be suitable for modeling not only the seven TM $\alpha$ bundle, but also for modeling peripheral secondary structure elements, such as the $\beta$ hairpin in EL2 and the C-terminal helix 8.

## REFERENCES

1. Gaibelet, G., Meilhoc, E., Riond, J., Saves, I., Exner, T., Liaubet, L., Nurnberg, B., Masson, J. M., and Emorine, L. J. (1999) Nonselective coupling of the human $\mu$-opioid receptor to multiple inhibitory G-protein isoforms, *Eur. J. Biochem. 261*, 517–523.

2. Shippenberg, T. S., and Elmer, G. I. (1998) The neurobiology of opiate reinforcement, *Crit. Rev. Neurobiol. 12*, 267–303.

3. Palczewski, K., Kumasaka, T., Hori, T., Behnke, C. A., Motoshima, H., Fox, B. A., Le Trong, I., Teller, D. C., Okada, T., Stenkamp, R. E., Yamamoto, M., and Miyano, M. (2000) Crystal structure of rhodopsin: A G protein-coupled receptor, *Science 289*, 739–745.

4. Flower, D. R. (1999) Modelling G-protein-coupled receptors for drug design, *Biochim. Biophys. Acta 1422*, 207–234.

5. Metzger, T. G., Paterlini, M. G., Portoghese, P. S., and Ferguson, D. M. (1996) An analysis of the conserved residues between

halobacterial retinal proteins and G-protein coupled receptors: Implications for GPCR modeling, *J. Chem. Inf. Comput. Sci. 36*, 857−861.

6. Strahs, D., and Weinstein, H. (1997) Comparative modeling and molecular dynamics studies of the $\delta$-, $\kappa$-, and $\mu$-opioid receptors, *Protein Eng. 10*, 1019−1038.

7. Alkorta, I., and Loew, G. H. (1996) A 3D model of the $\delta$-opioid receptor and ligand−receptor complexes, *Protein Eng. 9*, 573−583.

8. Subramanian, G., Paterlini, M. G., Portoghese, P. S., and Ferguson, D. M. (2000) Molecular docking reveals a novel binding site model for fentanyl at the $\mu$-opioid receptor, *J. Med. Chem. 43*, 381−391.

9. Filizola, M., Carteni-Farina, M., and Perez, J. J. (1999a) Molecular modeling study of the differential ligand−receptor interaction at the $\mu$-, $\delta$-, and $\kappa$-opioid receptors, *J. Comput.-Aided Mol. Des. 13*, 397−407.

10. Filizola, M., Laakkonen, L., and Loew, G. H. (1999b) 3D modeling, ligand binding, and activation studies of the cloned mouse $\delta$-, $\mu$-, and $\kappa$-opioid receptors, *Protein Eng. 12*, 927−942.

11. Iadanza, M., Holtje, M., Ronsisvalle, G., and Holtje, H. D. (2002) $\kappa$-opioid receptor model in a phospholipid bilayer: Molecular dynamics simulation, *J. Med. Chem. 45*, 4838−4846.

12. Pogozheva, I. D., Lomize, A. L., and Mosberg, H. I. (1997) The transmembrane 7-$\alpha$-bundle of rhodopsin: Distance geometry calculations with hydrogen bonding constraints, *Biophys. J. 72*, 1963−1985.

13. Pogozheva, I. D., Lomize, A. L., and Mosberg, H. I. (1998) Opioid receptor three-dimensional structures from distance geometry calculations with hydrogen bonding constraints, *Biophys. J. 75*, 612−634.

14. Lomize, A. L., Pogozheva, I. D., and Mosberg, H. I. (1999) Structural organization of G-protein-coupled receptors, *J. Comput.-Aided Mol. Des. 13*, 325−353.

15. Teller, D. C., Okada, T., Behnke, C. A., Palczewski, K., and Stenkamp, R. (2001) Advances in the determination of a high-resolution three-dimensional structure of rhodopsin, a model of G-protein-coupled receptors (GPCRs), *Biochemistry 40*, 7761−7772.

16. Ballesteros, J. A., Shi, L., and Javitch, J. A. (2001) Structural mimicry in G protein-coupled receptors: Implications of the high-resolution structure of rhodopsin for structure−function analysis of rhodopsin-like receptors, *Mol. Pharmacol. 60*, 1−19.

17. Oliveira, L., Hulsen, T., Hulsik, D. L., Paiva, A. C. M., Vriend, G. (2002) Modelling G protein-coupled receptors, http://www.cmbi.kun.nl/7tm/articles/2002_4.pdf.

18. Bissantz, C., Bernard, P., Hibert, M., and Rognan, D. (2003) Protein-based virtual screening of chemical databases. II. Are homology models of G-protein coupled receptors suitable targets? *Proteins 50*, 5−25.

19. Horn, F., Bettler, E., Oliveira, L., Campagne, F., Cohen, F. E., and Vriend, G. (2003) GPCRDB information system for G protein-coupled receptors, *Nucleic Acids Res. 31*, 294−297.

20. Decaillot, F. M., Befort, K., Filliol, D., Yue, S., Walker, P., and Kieffer, B. L. (2003) Opioid receptor random mutagenesis reveals a mechanism for G protein-coupled receptor activation, *Nat. Struct. Biol. 10*, 629−636.

21. Chaturvedi, K., Christoffers, K. H., Singh, K., and Howells, R. D. (2000) Structure and regulation of opioid receptors, *Biopolymers 55*, 334−346.

22. Huang, P., Li, J., Chen, C., Visiers, I., Weinstein, H., and Liu-Chen, L. Y. (2001) Functional role of a conserved motif in TM6 of the rat $\mu$-opioid receptor: Constitutively active and inactive receptors result from substitutions of Thr6.34(279) with Lys and Asp, *Biochemistry 40*, 13501−13509.

23. Mosberg, H. I., and Fowler, C. B. (2002) Development and validation of opioid ligand−receptor interaction models: The structural basis of $\mu$ vs $\delta$ selectivity, *J. Pept. Res. 60*, 329−335.

24. Baker, D., and Sali, A. (2001) Protein structure prediction and structural genomics, *Science 294*, 93−96.

25. Eswar, N., John, B., Mirkovic, N., Fiser, A., Ilyin, V. A., Pieper, U., Stuart, A. C., Marti-Renom, M. A., Madhusudhan, M. S., Yerkovich, B., and Sali, A. (2003) Tools for comparative protein structure modeling and analysis, *Nucleic Acids Res. 31*, 3375−3380.

26. John, B., and Sali, A. (2003) Comparative protein structure modeling by iterative alignment, model building, and model assessment, *Nucleic Acids Res. 31*, 3982−3992.

27. Riek, R. P., Rigoutsos, I., Novotny, J., and Graham, R. M. (2001) Non-$\alpha$-helical elements modulate polytopic membrane protein architecture, *J. Mol. Biol. 306*, 349−362.

28. Keefe, L. J., Sondek, J., Shortle, D., and Lattman, E. E. (1993) The $\alpha$ aneurism: A structural motif revealed in an insertion mutant of staphylococcal nuclease, *Proc. Natl. Acad. Sci. U.S.A. 90*, 3275−3279.

29. Beck, M., Sakmar, T. P., and Siebert, F. (1998) Spectroscopic evidence for interaction between transmembrane helices 3 and 5 in rhodopsin, *Biochemistry 37*, 7630−7639.

30. Elling, C. E., Nielsen, S. M., and Schwartz, T. W. (1995) Conversion of antagonist binding site to metal-ion site in the tachykinin NK-1 receptor, *Nature 374*, 74−77.

31. Elling, C. E., and Schwartz, T. W. (1996) Connectivity and orientation of the seven helical bundle in the Tachykinin NK$_1$ receptor probed by zinc site engineering, *EMBO J. 15*, 6213−6219.

32. Holst, B., Elling, C. E., and Schwartz, T. W. (2000) Partial agonism through a zinc-ion switch constructed between transmembrane domains III and VII in the tachykinin NK$_1$ receptor, *Mol. Pharmacol. 58*, 263−270.

33. Thirstrup, K., Elling, C. E., Hjorth, S. A., and Schwartz, T. W. (1996) Construction of a high-affinity zinc-switch in the $\kappa$-opioid receptor, *J. Biol. Chem. 271*, 7875−7878.

34. Elling, C. E., Thirstrup, K., Holst, B., and Schwartz, T. W. (1999) Conversion of agonist site to metal-ion chelator site in the $\beta$2-adrenergic receptor, *Proc. Natl. Acad. Sci. U.S.A. 96*, 12322−12327.

35. Berg, J. M., and Shi, Y. (1996) The galvanization of biology: A growing appreciation for the roles of zinc, *Science 271*, 1081−1085.

36. Glusker, J. P. (1991) Structural aspects of metal liganding to functional groups in proteins, *Adv. Protein Chem. 42*, 1−76.

37. Christianson, D. W. (1991) Structural biology of zinc, *Adv. Protein Chem. 42*, 281−355.

38. Mansour, A., Hoversten, M., Taylor, L. P., Watson, S. J., and Akil, H. (1995) The cloned $\mu$, $\delta$, and $\kappa$ receptors and their endogenous ligands: Evidence for two opioid peptide recognition cores, *Brain Res. 700*, 89−98.

39. Bradford, M. M. (1976) A rapid and sensitive method for the quantitation of microgram quantities of protein utilizing the principle of protein-dye binding, *Anal. Biochem. 72*, 248−254.

40. Berman, H. M., Westbrook, J., Feng, Z., Gilliland, G., Bhat, T. N., Weissig, H., Shindyalov, I. N., and Bourne, P. E. (2000) The Protein Data Bank, *Nucleic Acids Res. 28*, 235−242.

41. Chaturvedi, K., Shahrestanifar, M., and Howells, R. D. (2000) $\mu$-Opioid receptor: Role for the amino terminus as a determinant of ligand binding affinity, *Mol. Brain Res. 76*, 64−72.

42. Blaber, M., Zhang, X.-J., Lindstrom, J. D., Pepiot, S. D., Baase, W. A., and Matthews, B. W. (1994) Determination of $\alpha$-helix propensity within the context of a folded protein. Sites 44 and 131 in bacteriophage T4 lysozyme, *J. Mol. Biol. 235*, 600−624.

43. Guntert, P., and Wuthrich, K. (1991) Improved efficiency of protein structure calculations from NMR data using the program DIANA with redundant dihedral angle constraints, *J. Biomol. NMR 1*, 447−456.

44. Minami, M., Nakagawa, T., Seki, T., Onogi, T., Aoki, Y., Katao, Y., Katsumata, S., and Satoh, M. (1996) A single residue, Lys108, of the $\delta$-opioid receptor prevents the $\mu$-opioid-selective ligand [D-Ala2,N-MePhe4,Gly-ol5]enkephalin from binding to the $\delta$-opioid receptor, *Mol. Pharmacol. 50*, 1413−1422.

45. Javitch, J. A., Ballesteros, J. A., Chen, J., Chiappa, V., and Simpson, M. M. (1999) Electrostatic and aromatic microdomains within the binding-site crevice of the D2 receptor: Contributions of the second membrane-spanning segment, *Biochemistry 38*, 7961−7968.

46. Yang, Y., Dickinson, C., Haskell-Luevano, C., and Gantz, I. (1997) Molecular basis for the interaction of [Nle4,D-Phe7]melanocyte stimulating hormone with the human melanocortin-1 receptor, *J. Biol. Chem. 272*, 23000−23010.

47. Yang, Y. K., Fong, T. M., Dickinson, C. J., Mao, C., Li, J. Y., Tota, M. R., Mosley, R., Van Der Ploeg, L. H., and Gantz, I. (2000) Molecular determinants of ligand binding to the human melanocortin-4 receptor, *Biochemistry 39*, 14900−14911.

48. Zhang, P., Johnson, P. S., Zollner, C., Wang, W., Wang, Z., Montes, A. E., Seidleck, B. K., Blaschak, C. J., and Surratt, C. K. (1999) Mutation of human $\mu$-opioid receptor extracellular "disulfide cysteine" residues alters ligand binding but does not

Fowler et al.

prevent receptor targeting to the cell plasma membrane, *Brain Res. Mol. Brain Res. 72*, 195−204.

49. Hjorth, S. A., Thirstrup, K., Grandy, D. K., and Schwartz, T. W. (1995) Analysis of selective binding epitopes for the $\kappa$-opioid receptor antagonist nor-binaltorphimine. *Mol. Pharmacol. 47*, 1089−1094.

50. Tejwani, G. A., and Hanissian, S. H. (1990) Modulation of $\mu$-, $\delta$-, and $\kappa$-opioid receptors in rat brain by metal ions and histidine, *Neuropharmacology 29*, 445−452.

51. Bot, G., Blake, A. D., Li, S., and Reisine, T. (1998) Mutagenesis of a single amino acid in the rat $\mu$-opioid receptor discriminates ligand binding, *J. Neurochem. 70*, 358−365.

52. Xu, H., Lu, Y.-F., Partilla, J. S., Zheng, Q.-X., Wang, J.-B., Brine, G. A., Carroll, F. I., Rice, K. C., Chen, K.-X., Chi, Z.-Q., and Rothman, R. B. (1999) Opioid peptide receptor studies, 11: Involvement of Tyr148, Trp318, and His319 of the rat $\mu$-opioid receptor in binding of $\mu$-selective ligands, *Synapse 32*, 23−28.

53. Shi, L., and Javitch, J. (2004) The second extracellular loop of the dopamine D2 receptor lines the binding-site crevice, *Proc. Natl. Acad. Sci. U.S.A. 101*, 440−445.

54. Hanissian, S. H., and Tejwani, G. A. (1988) Histidine abolishes the inhibition by zinc of naloxone binding to opioid receptors in rat brain, *Neuropharmacology 27*, 1145−1149.

55. Swaminath, G., Lee, T. W., and Kobilka, B. (2003) Identification of an allosteric binding site for $Zn^{2+}$ on the $\beta$2 adrenergic receptor, *J. Biol. Chem. 278*, 352−356.

56. Holst, B., Elling, C. E., and Schwartz, T. W. (2002) Metal ion-mediated agonism and agonist enhancement in melanocortin MC1 and MC4 receptors, *J. Biol. Chem. 277*, 47662−47670.

57. Holst, B., and Schwartz, T. W. (2003) Molecular mechanism of agonism and inverse agonism in the melanocortin receptors: Zn(2+) as a structural and functional probe, *Ann. N.Y. Acad. Sci. 994*, 1−11.

58. Rosenkilde, M. M., Lucibello, M., Holst, B., and Schwartz, T. W. (1998) Natural agonist enhancing bis-His zinc-site in transmembrane segment V of the tachykinin NK3 receptor, *FEBS Lett. 439*, 35−40.

59. Sheikh, S. P., Zvyaga, T. A., Lichtarge, O., Sakmar, T. P., and Bourne, H. R. (1996) Rhodopsin activation blocked by metal-ion-binding sites linking transmembrane helices C and F, *Nature 383*, 347−350.

60. Sheikh, S. P., Vilardarga, J. P., Baranski, T. J., Lichtarge, O., Iiri, T., Meng, E. C., Nissenson, R. A., and Bourne, H. R. (1999) Similar structures and shared switch mechanisms of the $\beta$2-adrenoceptor and the parathyroid hormone receptor. Zn(II) bridges between helices III and VI block activation, *J. Biol. Chem. 274*, 17033−17041.

61. Lagerstrom, M. C., Klovins, J., Fredriksson, R., Fridmanis, D., Haitina, T., Ling, M. K., Berglund, M. M., and Schioth, H. B. (2003) High affinity agonistic metal ion binding sites within the melanocortin 4 receptor illustrate conformational change of transmembrane region 3, *J. Biol. Chem. 278*, 51521−51526.

62. Klein-Seetharaman, J. (2002) Dynamics in rhodopsin, *ChemBioChem 3*, 981−986.

63. Javitch, J. A., Fu, D., and Chen, J. (1995) Residues in the fifth membrane-spanning segment of the dopamine D2 receptor exposed in the binding-site crevice, *Biochemistry 34*, 16433−16439.

64. Xu, W., Li, J., Chen, C., Huang, P., Weinstein, H., Javitch, J. A., Shi, L., de Riel, J. K., and Liu-Chen, L. Y. (2001) Comparison of the amino acid residues in the sixth transmembrane domains accessible in the binding-site crevices of $\mu$-, $\delta$-, and $\kappa$-opioid receptors, *Biochemistry 40*, 8018−8029.